Engineering Structures 32 (2010) 2300–2309

Contents lists available at ScienceDirect

Engineering Structures

journal homepage: www.elsevier.com/locate/engstruct

Obtaining optimal performance with reinforcement-free concrete highway bridge decks

Han-Ug Bae, Michael G. Oliva *, Lawrence C. Bank

Department of Civil and Environmental Engineering, University of Wisconsin-Madison, 2205 Engineering Hall, 1415 Engineering Drive, Madison, WI 53706, USA

ARTICLE INFO

Article history:
Received 18 July 2009
Received in revised form
16 March 2010
Accepted 2 April 2010
Available online 20 May 2010

Keywords:
Bridge
FEM analysis
Reinforcement-free decks
Punching shear
Precast girders
Prestressed girders
Bridge decks
Concrete decks
Compressive membrane action
Precast bridges

ABSTRACT

This article describes an application of nonlinear finite element modeling (FEM) and analysis in the selection of design details to provide desirable performance in reinforcement-free concrete highway bridge decks. The FEM approach was used to predict the ultimate capacity and failure modes of decks considered as constrained membranes. Lateral constraint of the deck (membrane) provides extra wheel load capacity for reinforcement-free bridge decks on bulb tee wide flanged concrete girders. The wide flange precast prestressed concrete girder sections currently used in bridges result in a shorter effective span for the bridge deck between the wide girder top flanges. The failure mode of concrete decks on these girders with wheel loading is expected to be punching shear. The shear forces from the vehicle wheel loads in the reinforcement-free bridge deck are designed to be carried by compressive membrane action without using reinforcing in the concrete. The compressive membrane action is enhanced by the natural lateral stiffness of the wide girder flanges and by tying adjacent girders together with steel rods placed between the webs. An experimental study of a restrained deck element was performed to identify the failure mode and to use as a basis for verifying the nonlinear properties used in finite element analysis. A parametric study using nonlinear finite element analysis was performed to investigate the factors affecting the ultimate capacity and the failure modes of reinforcement-free bridge decks on wide flange precast girders and to provide a basis for selecting desirable design details.

1. Introduction

Transportation agencies are pursuing means for more rapid construction and longer durability of infrastructure components while trying to reduce initial and life-cycle costs. For highway bridges this is often achieved by using precast concrete. Efforts to improve durability have recently been realized by replacing corrosion susceptible steel reinforcing with alternate composite materials. Accelerated construction, improved durability and reduced cost for bridge decks exposed to corrosive salts are proposed in this discussion by completely removing reinforcing from the deck.

The Wisconsin Department of Transportation recently developed two new wide flange precast prestressed concrete girder (bulb tee) sections (54W and 72W girders) for highway bridges to improve span effectiveness compared to conventional AASHTO "I" girder sections. The moment of inertia of the wide flange girder increases due to the wider top flange and the feasible span increases. Many other transportation authorities are already using similar girders. Since the clear span of the deck, between girder flanges, is much shorter than deck spans between "I" girders, it is reasonable to suspect that the deck will perform differently. Testing of a 203 mm thick bridge deck built over the Wisconsin precast prestressed wide flange girders (Wisconsin 54W girders) conducted during a previous study [1] indicated that the bridge deck strength, over 890 kN of wheel load, far exceeded that needed to resist the AASHTO [2] factored design wheel load of 160 kN. Load resistance by compressive membrane action in the deck (also known as arching action) might have been responsible for the excess capacity.

A new deck design method that accounted for the effects of lateral restraint was proposed by Oliva et al. [3] and results in reinforcement-free bridge decks. To prove the feasibility of the new design approach, a pilot bridge was designed and built in Wisconsin, USA. The design concept eliminated the need for conventional deck reinforcing, the labor involved in placing reinforcing, and eliminated the need for temporary formwork during deck construction—thereby achieving a more effective load carrying mechanism, rapid construction and cost efficiency.

The research described here was aimed at developing methods for obtaining accurate estimates of the strength of reinforcement-free bridge decks and using those methods to define desirable design details to be used in a design procedure.

The new design concept recognizes the increase in shear capacity that develops with compressive membrane action in a

* Corresponding author. Tel.: +1 608 262 7241; fax: +1 608 262 5199.
E-mail address: oliva@engr.wisc.edu (M.G. Oliva).

0141-0296/$ – see front matter © 2010 Elsevier Ltd. All rights reserved.
doi:10.1016/j.engstruct.2010.04.004

Notations

α_f	Coefficient for fracture energy given in Table 1 (N mm/mm^2)
β_f	Coefficient for crack opening given in Table 1
f_{ct}	Tensile stress of concrete (MPa)
f_{ctm}	Tensile strength of concrete (MPa)
G_f	Fracture energy (N mm/mm^2)
R	Deck restraint factor (N/mm^2)
T_c	Coefficient for the direct tensile strength of the concrete
w_1	Crack opening for $f_{ct} = 0.15 f_{ctm}$ (mm)
w_c	Crack opening for $f_{ct} = 0$ (mm)
w	Crack opening width (mm)

concrete deck. Improved lateral restraint of the deck, achieved by tying laterally stiff girders together with steel rods, further enhances the shear capacity. The rods may be at a typical spacing of 3000 mm and do not replace normal bracing or diaphragms. The ties only extend between adjacent girders and may be stepped in a skew deck; they are not prestressed. The design relies on polypropylene fiber reinforcing in the concrete to control early age shrinkage cracks. Fiber reinforced polymer (FRP) stay-in-place (SIP) panels are used as formwork and also serve as a crack control device if the panels develop composite action with the concrete. Additional information on the FRP SIP panels including stiffness, dimensions and aggregate coating can be found elsewhere [4].

Since compression membrane action does not develop sufficiently in cantilevered decks, bridges designed to take advantage of that action should not use decks cantilevered beyond the flange of the exterior girders. In continuous multi-span bridges longitudinal deck reinforcing may still be required over interior piers. A schematic of the reinforcement-free bridge deck on precast girders is shown in Fig. 1.

The failure mode of the reinforcement-free deck is shear punching when sufficient lateral restraint is provided. Finite element analysis was required to identify the factors affecting the ultimate capacity and failure mode of the reinforcement-free bridge decks as a basis for defining the design process.

In the research described here experimental testing of a restrained reinforcement-free bridge deck sub-assemblage was performed to identify the failure mode of the deck and was used as a basis for the development of an accurate nonlinear finite element model which accounts for both material and geometrical nonlinearity. A parametric study using nonlinear finite element analysis then investigated the factors affecting the ultimate capacity and failure mode of restrained reinforcement-free bridge decks on precast concrete wide flanged bulb tee girders. The results found in this research form a basis for the development and the verification of a general simplified design procedure for reinforcement-free bridge decks [5].

2. Compressive membrane action and punching shear capacity of restrained decks

Compressive membrane action occurs in a laterally (in plane) restrained concrete deck slab. The concept is illustrated in Fig. 2. As the deck slab approaches strength capacity, flexural cracks develop in the positive and negative moment regions due to bending caused by the wheel load. After flexural cracking in the tensile zones, a lateral compressive membrane force develops as the deck starts rotating at the flexural cracks and tries to resist the vertical wheel load with diagonal compressive struts between the load and the girders. Lateral resistance for the struts is provided by the lateral

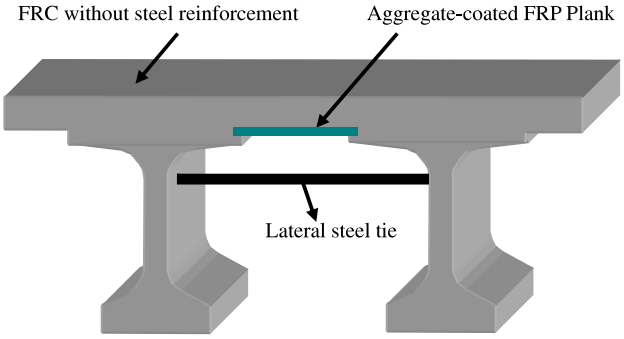

Fig. 1. Concept of the proposed deck system.

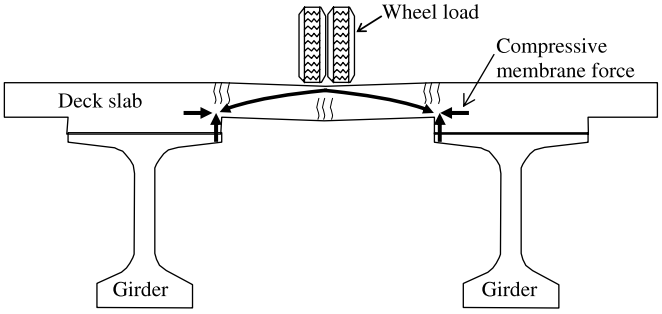

Fig. 2. Compressive membrane action in the cross-section of the bridge deck.

restraint from adjoining portions of the deck slab, the stiffness of any diaphragms between girders, and the lateral stiffness of the girders themselves. If a lateral tie is placed between the girder webs it can provide added lateral restraint. The development of this lateral resistance is referred to as compressive membrane action.

Researchers who initially recognized this phenomenon were Westgaard and Slater [6] and Ockleston [7]. They found that restrained concrete members had higher capacity than expected. Ockleston [8] found that compressive membrane action was responsible for strength enhancement. McDowell et al. [9], Park [10–12] and Hewitt and Batchelor [13] proposed methods to estimate the capacity enhancement in restrained concrete members. Several research studies examined theoretical models to predict the capacity and behavior of restrained concrete members [14–18]. Most of the studies concluded that the failure mode of the restrained member is punching shear but the mode is highly dependent on the degree of restraint. The studies focused on decks supported by steel or concrete "I" girders with longer clear spans, rather than the new bulb tee girders that possess a much higher lateral stiffness and result in a shorter clear deck span because of the wider top girder flange. None of the studies developed satisfactory design methods that accounted for both flexural and shear failure modes.

One of the applications where compressive membrane action has been utilized is in the development of steel-free bridge decks as proposed by Mufti et al. [19]. That concept of the steel-free bridge deck included removal of conventional steel reinforcing bars from the concrete in order to prevent corrosion of steel and deterioration of deck slabs subjected to deicing salts and environments. Steel straps between beams, externally welded at the tops of flanges of the beams, were used to provide added lateral restraint to the decks. Fiber reinforcing was used to control thermal and shrinkage cracks in the deck system [20]. Laboratory experiments proved that the steel-free deck system on steel beams, with fiber reinforced concrete and external steel straps for lateral restraint, had sufficient ultimate capacity for use in bridge decks [21,22].

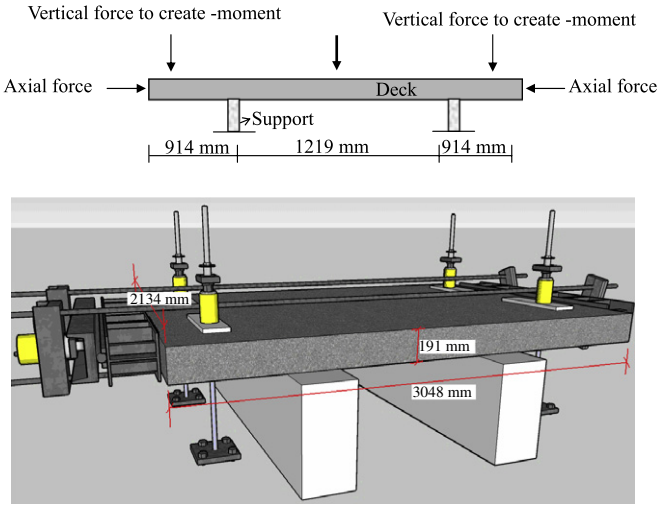

Fig. 3. Configuration of the restrained deck test.

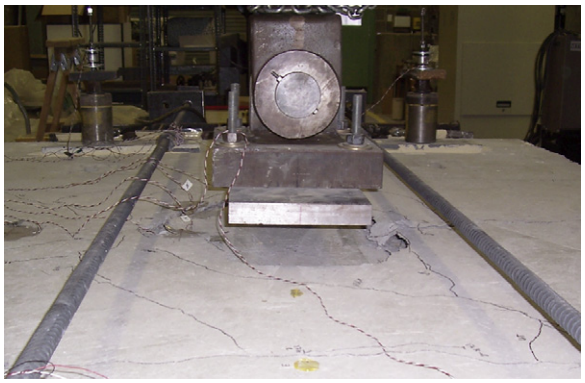

Fig. 4. Punching shear failure of the restrained deck test.

3. Restrained deck panel testing

Testing of a full scale deck panel with uniform confining force was conducted in the preliminary stage of this research to provide a basis for developing the FEM analysis method [23]. The deck test used controlled axial force to create the compressive membrane restraint and special vertical loads to induce the negative bending moment that would develop in a continuous deck over girders. A single patch load, to simulate a wheel, was applied at the middle of the 1219 mm deck clear span. The dimensions of the test slab were 2134 mm (width) × 3048 mm (length) × 191 mm (thickness). The configuration of the test is shown in Fig. 3.

The concrete of the test specimen was reinforced with 2.27 kg of polypropylene fibrillated and mono fiber per cubic meter (0.32% in volume fraction) to prevent plastic shrinkage cracking [24]. The uniaxial compressive strength of the concrete, found from cylindrical specimen testing, was 46.6 MPa. Though FRP SIP formwork was used in the pilot bridge construction, it was not included in the test in order to obtain the independent behavior of the restrained concrete alone.

The amount of axial restraint and negative moment applied at the slab ends during the test were determined from a preliminary analytic prediction of the behavior of a similar reinforcement-free deck on wide flange girders. Axial and vertical forces, to create the desired axial restraint and moment, were introduced by hydraulic jacks acting on the concrete as shown in Fig. 3. As the midspan wheel load was increased, the deck failed in punching shear as shown in Fig. 4 with an ultimate capacity of 474 kN.

This experiment verified the basic concept of compressive membrane action in developing a capacity well above the predicted failure load in flexure without reinforcing. The predicted failure load in flexure without reinforcing, calculated using AASHTO [2] strip method and ACI [25] equation for modulus of rupture of concrete assuming that the support condition of the deck is fully fixed is 224.6 kN. An unreinforced slab like this, without lateral restraint, would normally collapse immediately after initial flexural cracking at midspan. The test also showed that the failure mode of the deck was not flexure, but is in punching shear when sufficient lateral restraint is provided.

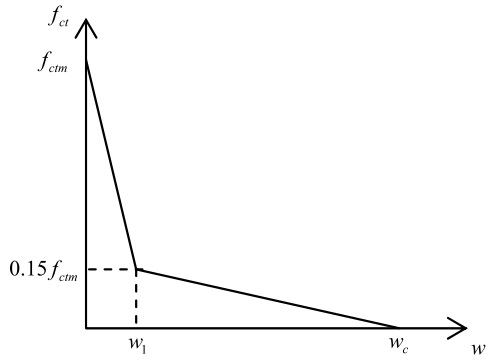

Fig. 5. Tensile strain softening plot (CEB-FIP model code 1990).

The behavior of the deck was compared to that from a nonlinear finite element prediction to prove the capability of the finite element analytic method. It was obvious that the result of the nonlinear finite element analysis would be highly dependent on the nonlinear material properties, i.e. tensile stiffening curve and tensile strength of the concrete. The proper values for those properties were found from the literature [26–29] except for the direct tensile strength of the concrete which will be described later. The properties were validated through the FEM deck simulation in comparison to the experimental results described in the next section.

4. FEM analysis of bridge deck

Finite element analysis was used to investigate the behavior of a series of reinforcement-free decks on wide flange concrete girders as various design parameters were modified. The analysis results from the accurate FEM approach could then serve as a basis for developing design guidelines and more simplified analytical methods that designers could apply.

4.1. Modeling properties

Hognestad equations were used to model the compressive stress versus strain relationship of the concrete [26]. The tensile modulus of elasticity of the deck, used before reaching tensile strength of the concrete, was assumed to be identical to the constant compressive modulus of elasticity of the concrete calculated from an American Concrete Institute (ACI) equation [25].

The strain softening curve of the concrete, when in tension after reaching the tensile strength of the concrete, was selected based on the CEB-FIP model code [27]. It is preferable to use displacement, instead of strain, for modeling the strain softening curve since the result is independent of element size in a FEM analysis when displacement is used as suggested by the software producer [28]. The code recommends using a strain softening curve shown in Fig. 5.

The methods for calculating w_1 and w_c are shown in Eq. (1).

$$G_f = \alpha_f \left(\frac{f_{\text{ctm}}}{f_{\text{ctm0}}}\right)^{0.7}, \quad f_{\text{ctm0}} = 10\,\text{MPa},$$
$$w_1 = \frac{2G_f}{f_{\text{ctm}}} - 0.15w_c, \quad w_c = \beta_f \frac{G_f}{f_{\text{ctm}}}. \tag{1}$$

Table 1
Coefficients α_f and β_f as functions of the maximum aggregate size (CEB-FIP model code 1990).

Maximum aggregate size (mm)	α_f (N mm/mm^2)	β_f
8	0.02	8
16	0.03	7
32	0.05	5

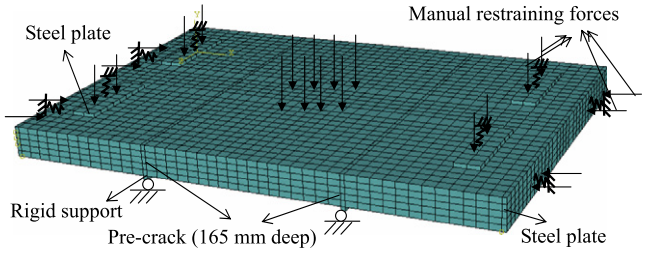

Fig. 6. Modeling of the restrained deck specimen.

The values for α_f and β_f in Table 1 are for plain concrete. When the concrete is reinforced by fibers the values increase. The increase of the coefficients α_f and β_f by adding fibers were assumed using existing experimental results from other researchers [29] and will be described later.

4.2. FEM analysis of the restrained deck test specimen

ABAQUS 6.6-1 [28] software was used for the FEM analysis. A full model of the test specimen was built and the "Hex 3D stress element with the linear geometric order option" and a "reduced integration scheme" were used to reduce the required time for running. The "Nonlinear effects of large displacement" option was selected since deformations would become large as failure is approached.

The test of the restrained deck was used to verify modeling parameters. Before the laboratory deck was tested to failure, sufficient loading was applied to develop flexural cracking in the negative moment region above the two supports. In the FEM model, 165 mm deep cracks that already existed in the deck from pre-loading were simulated at the negative moment regions of the deck.

Springs were used as boundary conditions where the actual deck restraining forces were introduced by steel rods. The manual restraining forces, in the horizontal and vertical directions, that were applied at the initial stage of the testing were located at the two nodes near the spring location.

The deck elements were 70 mm (width) × 70 mm (length) × 38 mm (thick) and 7024 elements were used in the model. The model and boundary conditions of the deck are shown in Fig. 6.

The coefficients α_f and β_f, tension parameters to determine the tensile stress–displacement relationship for the plain concrete, were taken as 0.04 N mm/mm^2 and 6, respectively, from Table 1 since the maximum aggregate size used in the experiment was between 16 and 32 mm. These coefficients were then modified to account for the fiber content in the concrete as will be described.

The fracture energy and the final crack opening width for the concrete before failure increase due to the fiber reinforcement. The fiber used in the experiment was a blended type of polypropylene fibrillated fiber and mono fiber. 0.072% of the fiber by volume was micro fiber and 0.251% of the fiber by volume was macro fiber in the concrete of the test deck. The increase in the fracture energy and final crack opening width were calculated using existing experimental results [29].

The direct tensile strength of the concrete has been found to be proportional to $\sqrt{f_c'}$ as shown in Eq. (2).

$$f_{ctm} = T_c\sqrt{f_c'}. \quad (2)$$

Table 2
Details of the properties used for the restrained deck analyses.

Analysis ID	T_c	w_1 (mm)	w_c (mm)	α_f (N mm/mm^2)	β_f
FEM-TC249	0.249	0.1499	0.6589	0.072	5.30
FEM-TC291	0.291	0.1280	0.5669	0.072	5.32
FEM-TC332	0.332	0.1120	0.4971	0.072	5.33

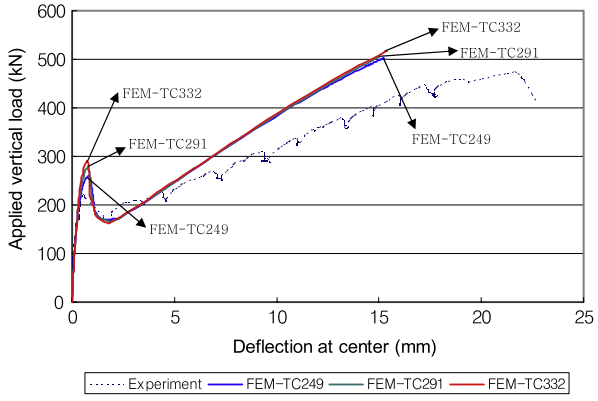

Fig. 7. Load versus displacement plots from FEM analyses and experiment.

The split-cylinder tensile strength has been found to be $0.498\sqrt{f_c'}$ to $0.581\sqrt{f_c'}$ for normal weight concrete [30]. The direct tensile strength of the normal weight concrete is 50%–70% of the split-cylinder tensile strength [30]. Therefore, the direct tensile strength of the concrete can be calculated using $T_c = 0.249$–0.407. To find an appropriate value for T_c which matched the experimental results of the restrained deck, three sets of FEM analyses were planned using $T_c = 0.249$, 0.291 and 0.332 bracketing the range given above. The analysis with the higher T_c was not performed since the results agreed well when T_c was 0.291.

The tensile strain softening properties of the concrete in the analyses are listed in Table 2. The predicted load versus deflection plot using the properties in Table 2 are shown in Fig. 7 with a comparison to the experimental result. The positive moment cracking load level and ultimate capacity obtained are listed in Table 3.

The sudden drop in capacity of Fig. 7 and Table 3 show that the FEM closely predicted the positive moment cracking force and the peak of the curve in Fig. 7 shows a good match with the measured ultimate strength capacity of the deck. The ratios of the FEM-TC291 analysis result to the experimental result for the positive moment cracking force and the ultimate strength capacity of the deck are 1.01 and 1.07, respectively. It is, however, stiffer than the actual test slab after cracking has developed. The average slopes of the load–displacement relationship after cracking for the FEM-TC291 analysis and the experiment were 24.49 kN/mm and 18.06 kN/mm, respectively. This is likely due to limited discrete cracking in the FEM model with deformation concentrated in a few cracks, while the actual test slab had more random and distributed cracking that created extra softening. The tensile stress–displacement relationship for the concrete used for the FEM-TC291 analysis is shown in Fig. 8.

After the initiation of a positive moment crack at the center of the deck span under the load, the crack immediately propagated to both side edges of the deck and the applied load dropped in the experiment. Additional loading was required in the FEM analysis before the crack propagated to the edges, which created the small difference in load levels at the first peak in Fig. 7.

The load capacity increases, after the cracking, as the compressive membrane action develops. The final failure mode in the analysis and the test was punching shear near the loading location. The FEM predicted diagonal shear crack occurred when the applied

Table 3
Cracking load level and ultimate capacity of the restrained deck from FEM and experiment.

	Positive moment cracking load level (kN)	Positive moment cracking load level (FEM/experiment)	Ultimate capacity (kN)	Ultimate capacity (FEM/experiment)
Experiment	221.29	–	473.75	–
FEM-TC249	206.87	0.93	501.80	1.06
FEM-TC291	223.26	1.01	505.75	1.07
FEM-TC332	251.10	1.13	516.82	1.09

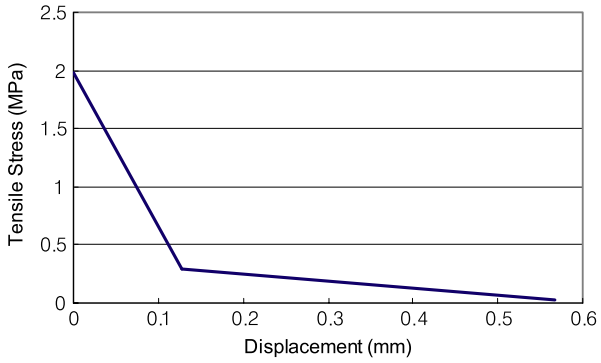

Fig. 8. Tensile stress–displacement relationship of concrete used for FEM-TC291.

load level was near the ultimate load in the analysis. The tensile plastic strain vectors in Fig. 9 show the amount of tensile strain increase after reaching ultimate tensile stress, and the direction. The diagonal cracking is perpendicular to the tension plastic strain vectors. The cracking predicted by the analysis compared closely with the cracking noted in the test specimen. The tensile plastic strain vectors shown in Fig. 9 are intentionally limited to only those near the shear cracking region.

The total axial restraining force and the vertical restraining force at one end of the deck from the analysis FEM-TC291 are compared to the experimental results in Fig. 10. The restraining forces from the experiments show good agreement with the FEM analysis value at the initial loading stage. After the positive moment crack occurs the forces from the FEM analysis are 15%–20% higher compared to the experimental values, for a given wheel load, indicating that the FEM model appears to develop more restraint than the actual test specimen. This is consistent with the smaller displacements of Fig. 7 and higher stiffness due to less cracking in the FEM model.

While the FEM predictions do not perfectly match the stiffness of the actual non-linear slab after cracking and as the ultimate capacity is approached, the analysis does give a good prediction of the strength capacity, failure mode, and failure surface. For purposes of strength prediction the FEM method is considered accurate.

4.3. Parametric study of bridge decks on wide flange girders

A FEM parametric study including variations of girder tie location, and deck restraint was performed, using the concrete properties identified above but with a different concrete strength, to evaluate the behavior of various deck designs. Since the FRP SIP formwork was not selected to provide strength, but rather to act only as forming and for crack control, it was purposely excluded in the FEM model. The forming has been shown to actually participate in providing strength [4], ignoring it will provide a conservative strength estimate. Decks on Wisconsin 54W girders (Fig. 11) were selected for the parametric study.

Ninety four separate analyses predicting the ultimate capacity of a deck with 27.6 MPa concrete compressive strength and 2.27 kg/m^3 of synthetic fibers, as expected to be used in actual bridge decks, were conducted. For the concrete in tension the T_c value was assumed as 0.291 since the fiber volume content

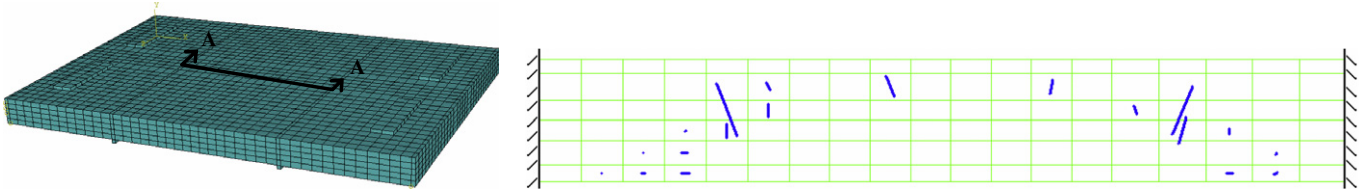

(a) FEM modeling. (b) Section A–A.

Fig. 9. Tensile plastic strain vectors of the restrained deck from FEM-TC291.

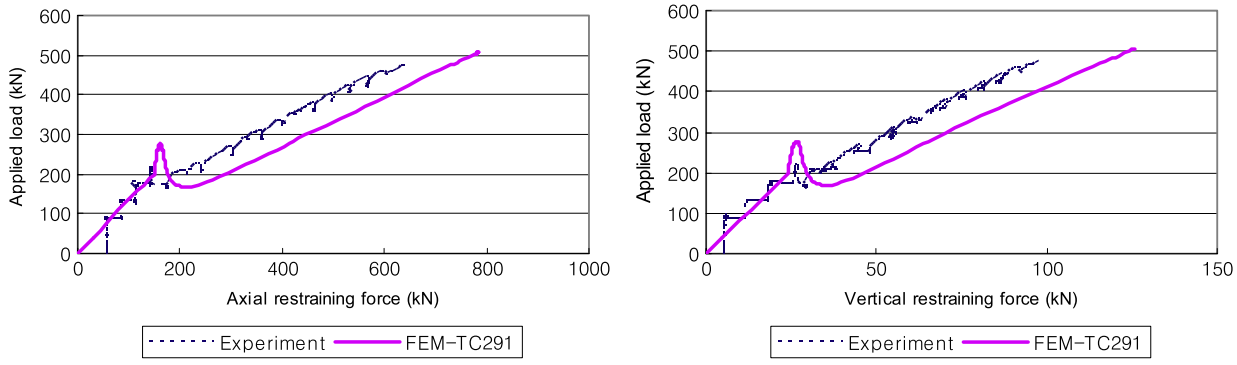

(a) Axial restraining force. (b) Vertical restraining force.

Fig. 10. Load versus restraining force plots for the experiment and FEM-TC291.

Table 4
Details of the tensile properties used for the FEM parametric study.

Property ID	T_c	w_1 (mm)	w_c (mm)	α_f (N mm/mm^2)	β_f
Parametric study	0.291	0.1153	0.5104	0.072	5.32

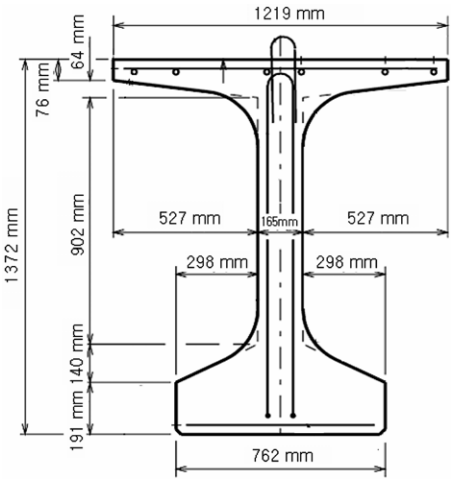

Fig. 11. Wisconsin 54W girder dimensions.

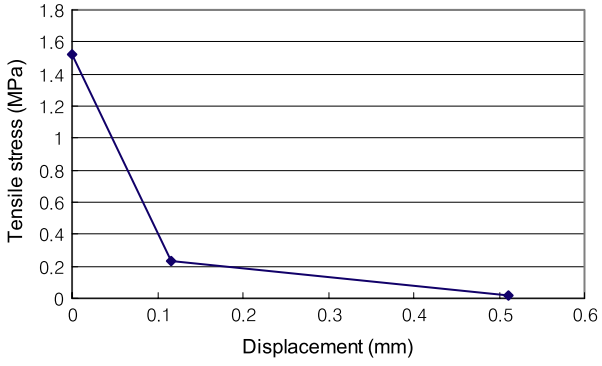

Fig. 12. Tensile stress–displacement relationship of the concrete in the parametric study.

and the mix of the concrete were assumed to be identical to the test deck. The tensile stress–displacement relationship and the corresponding variables used in the analysis are shown in Table 4 and Fig. 12.

The first factor found from the analyses was that the capacity or deformation behavior of the proposed deck system was not sensitive to the location (height) of the lateral steel ties in the webs

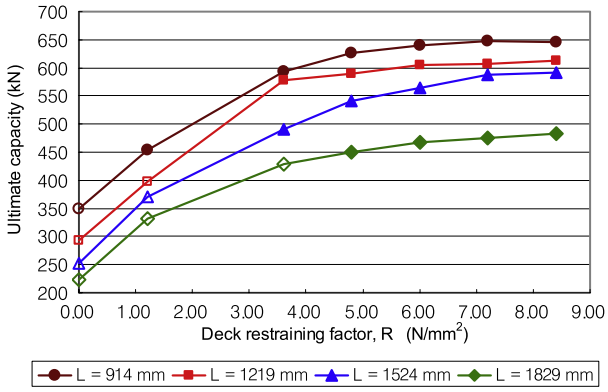

Fig. 14. Ultimate capacity versus deck restraining factor for 191 mm deep deck with 1829 mm lateral tie spacing (L is clear deck span).

of the girders. When the height of the tie was varied, from mid-web to bottom of top flange, the deck capacity remained virtually unchanged.

The effects of varying the other parameters, the deck span, thickness, tie spacing and tie cross-section area, are complicated to distinguish and judge separately. Dimensional analysis was used to reduce the number of parameters that needed to be varied. To help in judging the effects, a deck restraint factor (R) that combines parameters was proposed to compare behavior of the compressive membrane action and to use as a basis for design. (Eq. (3) in Box I).

The R parameter might be considered as representative of the tie "restraint" applied to the deck that will produce an increase in the shear strength. The deck restraint factor is proportional to the axial stiffness (area × modulus) of the lateral steel tie between girders and the thickness of the deck. Both of these factors represent a source of restraint around a possible punching shear failure surface. R is inversely proportional to the center to center spacing of the girders (length of the tie) and spacing of the lateral steel ties along the length of the girder as shown in Eq. (3), both items that could decrease the restraint as they grow larger.

FEM analyses were performed for bridges with 191 mm or 229 mm thick decks and 1829 to 3048 mm spacing of lateral steel ties. The clear span of the deck, between girder flanges, varied from 914 to 1829 mm. The resulting R factor varied from 0 to 8.40 N/mm^2 (low restraint to very large restraint).

The deck had two spans and was assumed to be attached compositely over three girders in the FEM model. The wheel load was applied in one deck span, to simulate load on a deck span adjacent to the bridge's exterior girder. A typical model with a clear deck span of 1524 mm, a 191 mm deck depth and a spacing between lateral steel ties of 1829 mm is shown in Fig. 13.

The results of the analyses are shown in Figs. 14–17. The plot points with solid symbols in the figures indicate predicted

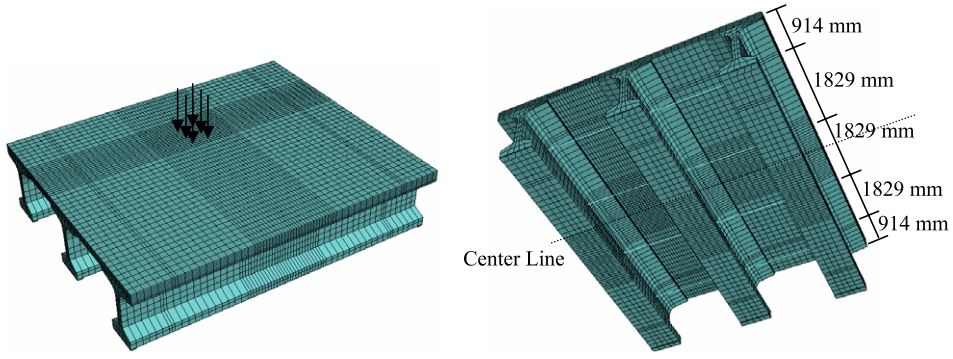

(a) Top view. (b) Bottom view.

Fig. 13. Modeling of the bridge for parametric study.

$$R = \frac{\text{axial stiffness of the lateral steel tie (N/mm)} \times \text{thickness of deck (mm)}}{\text{center to center spacing of girders (mm)} \times \text{spacing of lateral steel tie (mm)}} \quad (3)$$

Box I.

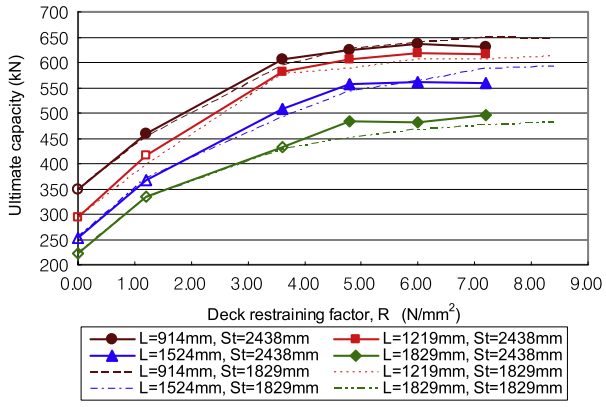

Fig. 15. Ultimate capacity versus deck restraining factor for 191 mm deep decks with 2438 mm and 1829 mm lateral tie spacing (L is clear deck span, St is tie spacing).

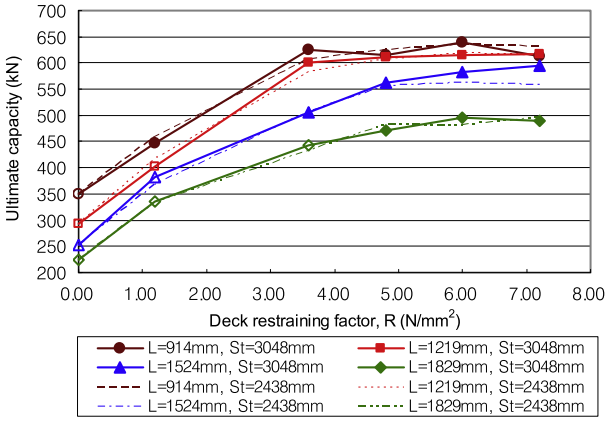

Fig. 16. Ultimate capacity versus deck restraining factor for 191 mm deep deck with 3048 mm and 2438 mm lateral tie spacing (L is clear deck span, St is tie spacing).

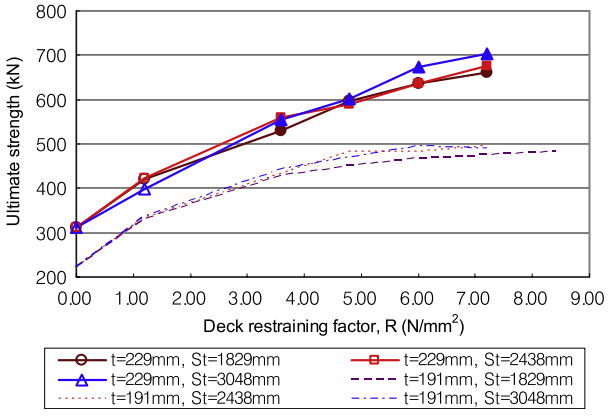

Fig. 17. Ultimate capacity versus deck restraining factor for 229 mm and 191 mm deep deck with 1829 mm clear deck span (t is deck depth, St is tie spacing).

punching failure of the deck, while hollow symbols indicate flexural failure of the deck. When the deck started to lose its capacity and diagonal cracks developed, the failure mode in the FEM model of the deck was defined as a punching failure. When the deck started to lose its capacity without the occurrence of diagonal cracks, the failure mode of the deck was defined as a flexural failure.

There were two kinds of behavior in the deck when flexural failure occurred: (a) loss of load capacity when the compressive stress at the top concrete fiber of the positive moment region reached its ultimate compressive stress, and (b) instability failure of the deck with a sudden growth of the crack and snap-through. The instability failure would naturally occur after flexural cracking if the restraint is low.

From Fig. 14 (and the other figures) it appears that the failure mode changes from flexure to punching shear once a certain level of restraint exists (hollow plot symbol to filled symbol). It shows that providing restraint can appreciably increase the failure capacity. Beyond a certain level of restraint, however, the increase in capacity with additional restraint (increasing R) is modest. The improvement in ultimate strength is reduced for deck restraining factors (R) over 3 N/mm^2 and is minimal above 6.2 N/mm^2.

Figs. 15 and 16 show that for a given span length, deck thickness and restraint (R), the failure capacity does not change significantly with tie spacing varying from 1829 to 3048 mm (dashed lines versus solid lines). The decks with the same thickness and span had the same capacity when the spacing of the ties was varied if the cross-sectional area of the tension ties (and axial stiffness) was modified to keep the deck restraint factor "R" constant.

This effect may be more evident in Fig. 17 where capacities for two different deck thicknesses are shown. For a constant deck thickness, the capacity is the same for any of the three different tie spacings as long as the same value of R is provided. Deck thickness, however, is seen to have a clear effect on the strength capacity. This would naturally occur because the compressive strut in the deck has a larger vertical angle, and larger vertical load resisting component, in a thicker deck.

In summary, it is evident that for a given amount of deck restraint, the strength drops as the span length increases, and gets larger as the deck thickness gets larger. For a given thickness and span, the strength depends on the girder tie stiffness per unit length of girder rather than just the tie spacing or tie size. Increasing the restraint, or "R" factor, above a value of approximately 6.2 N/mm^2 does not appreciably affect the strength. If the R factor is above 4.0 N/mm^2 the failure is likely to be shear punching, for lower values a flexural failure is likely to occur at a lower strength.

4.4. Application to other types of wide flange girders

Additional FEM analyses were performed for two other types of wide flange girders to investigate the relationship between ultimate strength of the wide flange girder and R factor. Wisconsin 72W girders and Washington state WS53 girders were selected (Fig. 18) for the additional FEM analyses.

The shape of the Wisconsin 72W girder is identical to the Wisconsin 54W girder except for the height of the web. Washington State WS53 girder flanges are joined together to form a complete superstructure for the bridge without casting a separate deck. The top flanges of the girders function as the deck. The center to center spacing of the girders is typically 1219 to 1829 mm. 1829 mm center to center spacing was selected for the FEM analyses. The flanges are joined together at the deck level using one of the two options. The keyway at the flange edges is completely filled with concrete grout, or steel flange ties are welded and then the keyway is filled with concrete grout. The Washington State WS53 girders analyzed here are assumed to be

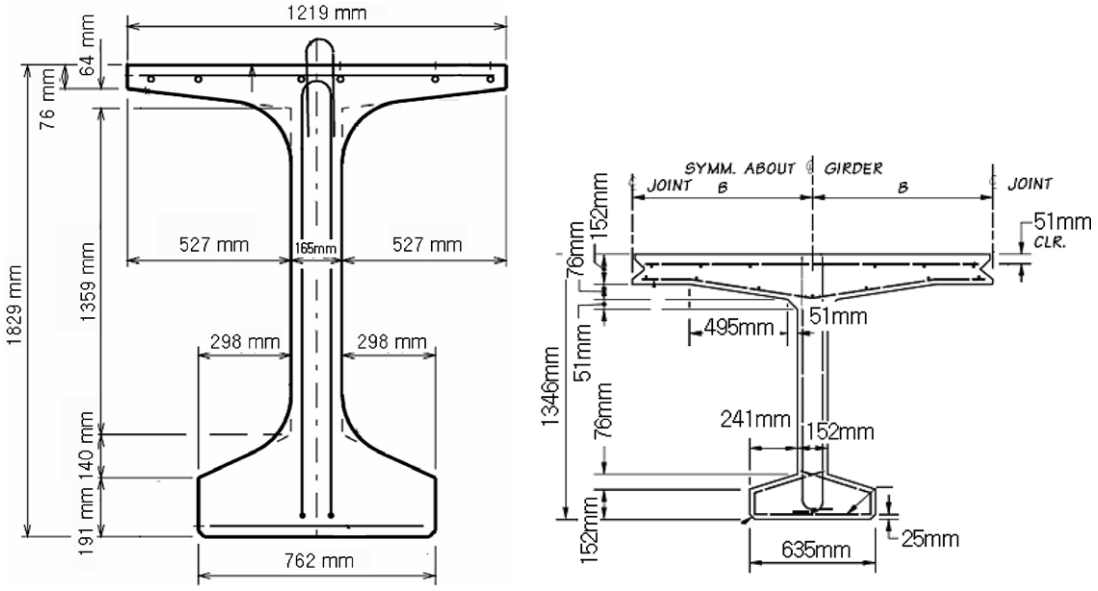

(a) Wisconsin 72W girder. (b) Washington State WS53 girder.

Fig. 18. Wisconsin 72W girder and Washington State WS53 girder dimensions.

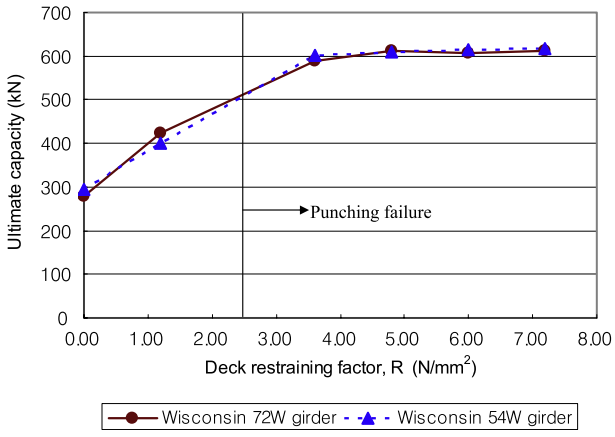

Fig. 19. Ultimate capacity versus deck restraining factor for the deck on Wisconsin 72W girders with a comparison to the deck on Wisconsin 54W girders.

joined using concrete grout only so that the concrete serves as the compression transfer mechanism. The property of the keyway was assumed be the same as the other top flange sections. The design compressive strength of the concrete for the Wisconsin 72W girders and Washington State WS53 girders are same as that of the previous Wisconsin 54W girder.

Six FEM analyses to estimate the capacity of the deck on Wisconsin 72W girders with various configurations of deck restraint were performed to compare the result with the deck on Wisconsin 54W girders. The modeling properties and scheme used to model the deck on Wisconsin 72W girders are identical to the deck on Wisconsin 54W girders since they have the same material properties. Deck thicknesses of 191 mm with 1219 mm long clear span, 3048 mm lateral steel tie spacing and various deck restraining factors were selected for the analysis. The ultimate capacities of the decks using the FEM analysis are shown in Fig. 19 and a comparison with the analysis results of the decks on Wisconsin 54W girders are included for the same configuration.

The FEM analysis results showed that the capacity of the deck on W72 and W54 girders did not show a noticeable difference. The factors influencing the deck restraining behavior with respect to the type of the girder are the displacement due to the weak axis bending and the torsion of the girder. The difference between the Wisconsin 72W girder and 54W girder in shape is in the height of the web. The increase in the height of the web contributes little toward the weak axis moment of inertia or the torsional stiffness even though it contributes significantly to the moment of inertia about the strong axis.

Six FEM analyses to estimate the capacity of the deck on Washington State WS53 girders with various configurations of deck restraint were performed. The modeling scheme used in the FEM model was identical to the deck on W54 girders. It is assumed that 2.27 kg/m^3 of synthetic fibers was used for the concrete at the top flange part of the girder which was the same amount of the fiber reinforcement that was assumed to be used for the deck on Wisconsin 54W girders. This small polypropylene fiber volume actually has little effect on the material strength. No other reinforcement was considered in the modeling for the top flange part of the girder. The concrete properties used in the modeling for the top flange part of the girder were assumed with the same procedure used for the Wisconsin 54W girders.

The predicted capacities of the deck portion of the Washington State WS53 girders, with various restraining factors, from the FEM analysis are shown in Fig. 20.

The failure mode was flexural failure when no lateral tension ties were used. The failure mode changed to punching failure when the lateral tension ties provided a deck restraining factor (R) higher than 1.2 N/mm^2. Increasing the restraint, or "R" factor, above a value of approximately 4.8 N/mm^2 does not appreciably affect the strength.

5. Summary and conclusions

Highway bridge decks that are on new types of wide flanged (bulb tee) precast concrete girders develop unusually high wheel load capacity due to lateral restraint provided to the deck. The deck develops compressive membrane action that reduces the likelihood of flexural failure and provides extra shear punching strength. Improved compressive restraint and compressive membrane action can be obtained in these bridge decks by using tension ties between girders that limit girder lateral movement and deck expansion.

An experimental study of a restrained reinforcement-free bridge deck sub-assemblage was performed. The test deck

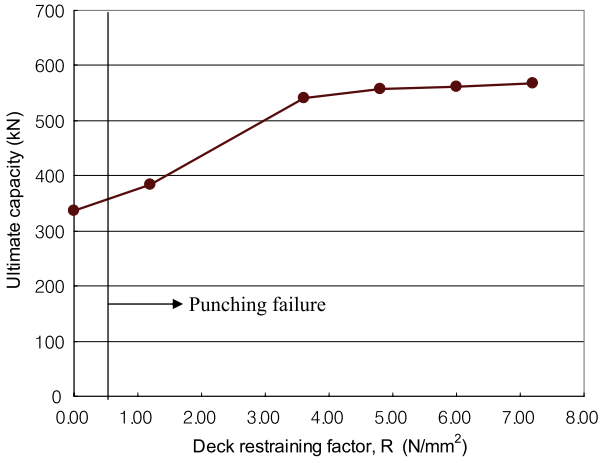

Fig. 20. Ultimate capacity versus deck restraining factor using for the deck portion of Washington State WS53 girders.

exhibited a punching shear mode of failure and was used as a basis for verification of a nonlinear finite element model.

A parametric study using nonlinear finite element analysis then investigated the factors affecting the ultimate capacity and failure mode of restrained reinforcement-free bridge decks on precast concrete wide flanged bulb tee girders such as the Wisconsin 54W, Wisconsin 72W and Washington State WS 53 girders.

The parametric study proved that providing lateral restraint for concrete deck slabs can change the failure mechanism from a flexural type to a punching shear type. Increasing the restraint increases the load carrying capacity of the slab up to a limiting value. Further restraint has a marginal impact on the slab's shear capacity. The deck restraint may be measured by a ratio of the product of slab thickness and girder tie stiffness to the product of slab span and girder tie spacing. For a given amount of restraint, the slab's capacity is higher for thicker decks and lower for decks with longer spans. The slab's capacity is not seriously affected by the girder tie spacing as long as the tie stiffness per foot of girder length remains constant.

The following conclusions regarding reinforcement-free bridge decks are made based on the combined experimental and analytical studies.

(1) The concept of compressive membrane action was verified. The failure mode of short span bridge decks under wheel loads is punching shear failure, rather than flexure, when sufficient lateral restraint is provided. A flexural failure or instability can occur without sufficient lateral restraint.
(2) Lateral tension ties between girders in reinforcement-free deck systems can serve as efficient lateral restraint devices for the deck. The ultimate capacity of the reinforcement-free deck, on a specific type of precast bridge girder, increases when girder ties provide added restraint. Strength increases of 75% to 135% can be developed, when sufficient ($R > 6.20$ N/mm^2) lateral tension restraint is provided in comparison to a deck without lateral tension ties.
(3) The improvement of the ultimate strength of the reinforcement-free bridge decks is minimal with an increase of the deck restraining factor (R) above 6.20 N/mm^2. This result can be used as a minimum restraint design limit for future bridge decks.
(4) The punching shear failure capacity of the restrained deck does not change significantly with increased girder tie spacing for a given span length, deck thickness and restraint (R).

This new approach to deck design and construction is intended to allow more rapid construction by elimination of internal reinforcement and by introducing stay-in-place formwork. It improves the deck durability by using non-corrosive materials such as FRP planks which control flexural cracking and non-metallic fibers in the deck which control plastic shrinkage cracking [24]. The material and labor costs in construction are reduced by elimination of internal reinforcement and the task of placing reinforcing as demonstrated in a pilot bridge. Design efficiency is improved by making the design process reflect the actual deck behavior. The FRP plank is susceptible to loss of strength under fire conditions, but as a stay-in-place formwork its contribution to strength is neglected and not required. The exposed ties between girders, however, are susceptible to loss of stiffness if a fire occurrs under a bridge but it is presumed that truck loading on the deck would not be present during a fire. After a fire the ties could be easily re-tightened to again serve or easily replaced while the bridge was closed to truck loading. Overall the new systems provide many advantages over current bridge deck design and construction methods.

Acknowledgements

This project was supported through funding provided by the Federal Highway Administration through the Wisconsin Department of Transportation under the Innovative Bridge Research and Construction program. The views expressed in the article are those of the authors and not the sponsoring organizations.

References

[1] Jacobson DA. Experimental and analytical study of fiber reinforced polymer (FRP) grid reinforced concrete bridge decking. M.S. thesis. Dept of Civil and Environmental Engineering. University of Wisconsin-Madison. 2004.
[2] AASHTO. AASHTO LRFD bridge design specifications. 4th ed. American Association of State Highway and Transportation Officials. 2008.
[3] Oliva MG, Bae H, Bank LC, Russell JS, Carter JW. et al. Design and construction of a reinforcement free concrete bridge deck on precast bulb tee girders. In: Proceedings of PCI/FHWA national bridge conference. CD-ROM. Phoenix (AZ). 22–24 October, 2007.
[4] Oliva M, Bae H, Bank L, Russell J, Yoo SW. FRP stay-in-place formwork for floor and deck construction. FRP Stay-in-Place Forms for Concrete Structures, ACI Special Publication 2008;SP-257:106–129.
[5] Bae H. Design of reinforcement-free bridge decks with wide flange prestressed precast concrete girders. Ph.D. thesis. Dept. of Civil and Environmental Engineering. University of Wisconsin-Madison. 2008.
[6] Westgaard HM, Slater WA. Moments and stresses in slabs. J Amer Concr Inst Proc ACI 1921;17:415–538.
[7] Ockleston AJ. Load tests on a three story reinforced concrete building in Johannesburg. Struct Eng 1955;33:304–22.
[8] Ockleston AJ. Arching action in reinforced concrete slabs. Struct Eng 1958;36:197–201.
[9] McDowell EI, McKee KE, Sevin E. Arching action theory of masonry walls. Proc Am Soc Civ Eng J Struct Div 1956;82(ST2):915-1–18.
[10] Park R. The ultimate strength and long-term behavior of uniformly loaded, two-way concrete slabs with partial lateral restraint at all edges. Mag Concr Res 1964;16(48):139–52.
[11] Park R. Ultimate strength of rectangular concrete slab under short-term uniform loading with edges restrained against lateral movement. Proc Inst Civ Eng 1964;28:125–50.
[12] Park R. The lateral stiffness and strength required to ensure membrane action at the ultimate load of a reinforced concrete slab-and-beam floor. Mag Concr Res 1965;17(50):29–38.
[13] Hewitt BE, Batchelor BdeV. Punching shear strength of restrained slabs. J Struct Div, ASCE 1975;101(ST9):1837–53.
[14] Kirkpatrick J, Rankin GIB, Long AE. Strength evaluation of M-beam bridge deck slabs. Struct Eng 1984;62B(3):60–8.
[15] Kuang JS, Moley CT. Punching shear behavior of restrained reinforced concrete slabs. ACI Struct J 1992;89(1):13–9.
[16] Kuang JS, Moley CT. A plasticity model for punching shear of laterally restrained slabs with compressive membrane action. Int J Mech Sci 1993;32(5):371–85.
[17] Rankin GIB, Long AE. Arching action strength enhancement in laterally-restrained slab strips. Proc Inst Civ Eng Struct Build 1997;122:461–7.
[18] Mufti AA, Newhook JP. Punching shear strength of restrained concrete bridge deck slabs. ACI Struct J 1998;95(4):375–81.
[19] Mufti AA, Bakht B, Jaeger LG. Fiber FRC deck slabs with diminished steel reinforcement. In: Proceedings of IABSE symposium. 1991. p. 388–9.
[20] Mufti AA, Jaeger LG, Bakht B, Wegner LD. Experimental investigation of fibre-reinforced concrete deck slabs without internal steel reinforcement. Can J Civ Eng 1993;20(3):398–406.

[21] Thorburn J, Mufti AA. Full-scale testing of externally reinforced FRC bridge decks on steel girders. In: Proceedings of annual conference of CSCE, vol. II. 1995. p. 543–52.
[22] Bakht B. Revisiting arching in deck slabs. Can J Civ Eng 1996;23(4):973–81.
[23] Georgieff P. Experimental and analytical investigation of reinforcement-free concrete bridge decks constructed with external tie bars. M.S. thesis. Dept of Civil and Environmental Engineering, University of Wisconsin-Madison. 2007.
[24] Naaman AE, Wongtanakitcharoen T, Hauser G. Influence of different fibers on plastic shrinkage cracking of concrete. ACI Mater J 2005;102(1):49–58.
[25] ACI-318. Building code requirements for structural concrete and commentary 318-05. American Concrete Institute, Committee 318. 2005.
[26] Park R, Paulay T. Reinforced concrete structures. John Wiley and Sons; 1975.
[27] CEP-FIP Model Code 1990. Switzerland: Thomas Telford; 1993.
[28] Hibbitt, Karlsson & Sorensen Inc. ABAQUS User's manual; 2004.
[29] Deng Z, Li J. Tension and impact behaviors of new type fiber reinforced concrete. Comput Concr 2007;4(1):19–32.
[30] Hassoun MN. Structural concrete. Prentice Hall; 2001.